Complementary Fluorescence Emission and Second Harmonic Spectra Improve Bilayer Characterization

Radha Ranganathan, Asher J. Burkin, and Miroslav Peric

Department of Physics, California State University Northridge, CA 91311, U.S.A.

Corresponding Author: Radha Ranganathan

radha.ranganathan@csun.edu

Keywords: Fluorescence, Laurdan, Phospholipid Bilayers, Fluorescence lineshape

Acknowledgements: The authors gratefully acknowledge NIH for their support through grant contract # 1SC3GM122499-01A1 and NSF MRI Grant 1626632. MP acknowledges NSF for RUI 1856746.

Abstract

Complementary investigation of Laurdan fluorescence emission and second harmonic (SH) spectra in nonpolar, protic and aprotic polar solvents and phospholipid bilayers was carried out. SH of spectra computed using methods familiar in electro spin resonance spectroscopy yielded better resolution. Spectra were fit to log-normal distributions. SH spectra showed presence of two emissions in protic polar and nonpolar solvents and in both bilayer gel and liquid phases and a single line in aprotic polar solvents. Each of the half maximal positions of each line in both homogenous solvents and bilayers, expresses similar linearity with peak position. This shared feature suggests planar and nonplanar Laurdan conformation respectively in the longer (red) and shorter (blue) wavelength emitting states. The weaker 432 nm blue line, not detected before in the gel phase, is distinguishable in the SH. Temperature trajectories of areas and peak positions of the individual lines bring new insight into the nature of lipid packing and evolution of domains, indicating inhomogeneous lipid packing even in the gel phase. The blue line identifies as emission from Laurdan in tighter packed regions and the dominant 445 - 448 nm red line in the gel phase shifting to 484 nm in the liquid phase as emission from Laurdan-water coupled states that are in varying stages of relaxation according to temperature and phase. Unexpected increase in the area of the blue line with temperature through the gel-liquid transition is consistent with coexisting low and high curvature domains and Laurdan's preference for less polar low curvature domains.

1.0 Introduction

Fluorescence spectra of complex molecules have long been recognized to better fit log-normal functions than Gaussians[1,2]. The log-normal distribution with peak height I_m and peak position k_m, as a function of wavenumber k, is:

$$\begin{cases} I(k) = I_m exp\left[-\frac{ln\,2}{ln^2(\rho)} ln^2\left(\frac{a-k}{a-k_m}\right)\right] & if\ k < a \\ I(k) = 0 & if\ k \geq a \end{cases} \quad (1)$$

The asymmetry of a log-normal function is parametrized by $\rho = \frac{k_m - k_{min}}{k_{max} - k_m}$, where k_{min} and k_{max} are the positions of half-maximal intensities. $a = k_m + \frac{(k_{max} - k_{\min)\rho}}{\rho^2 - 1}$ is the limiting wave number[2]. There are thus four parameters, including I_m, k_m, ρ, and a in fitting emission spectra to a single line. Spectra in various homogeneous solvents have been fit to single log-normal functions and the positions k_{min} and k_{max} of the half maxima were each found to bear a linear relation to the fluorescence peak position, k_m. These linear equations have been advanced as constraints to reduce the number of fit parameters when fitting spectra of the same fluorophore in systems like lipid bilayers and proteins where there are more elementary emissions than one[1,2]. However, a more refined fitting analysis involving the second harmonic of Laurdan spectra in several homogenous organic solvents and in lipid bilayers show departures from existing observations and in the application of constraint equations.

The solvatochromic property of Laurdan stems from its sensitivity to solvent polarity [3,4,2]. Laurdan fluorescence in homogeneous solvents has been reported to comprise of a single emission, and spectra are fitted to a single log-normal distribution. Evidence is presented here for the presence of more than one elementary emission in non-polar and protic polar and one emission line in aprotic polar solvents. While the linear relation between k_{min} or k_{max} vs k_m still holds for aprotic polar solvents, their use as constraints in fitting multiple line spectra observed in other solvents and lipid bilayers is not always viable.

Fluorescence measurements were conducted on several solvents belonging to the three classes: non-polar, aprotic polar, and protic polar. The second harmonic (SH) of the spectra were derived computationally using methods familiar in electron spin resonance (ESR) spectroscopy [5]. Complementary fitting of spectra and SH analysis is powerful in resolving ambiguities of fitting broad featureless shapes that are encountered in spectra of organic fluorophores because of better defined features available in the SH. Employing this approach found Laurdan emission to be described by a single emission line only in aprotic polar solvents. At least two lines are needed to fit the spectra in nonpolar and protic polar solvents and in lipid bilayer liquid as well as gel phases. Fit results include peak positions, linewidths, line asymmetry parameters (ρ), and areas of the individual lines. Spectral features derived from fitting bring new information on lipid packing in

bilayers and on the originating states of Laurdan emissions. Laurdan conformation and its hydrogen bonding capability, dipole interactions, and lipid packing appear to be at the center of solvent type and temperature dependence of emission characteristics.

2.0 Experiments

2.1. Materials and Methods: Homogeneous solvents listed in Tables 1 -3 in the supplemental information (SI) were from Sigma. Laurdan was obtained from Anaspec. Solutions of the phospholipids, DPPC and DSPC in chloroform, were from Avanti.

2.2. Sample Preparation: A stock solution of Laurdan in chloroform was first prepared. The required amount of Laurdan/chloroform for a final concentration of 7 μM was dried using nitrogen gas to evaporate the chloroform. Solvent was added to the dry film, and the mixture was stirred for a few hours. For phospholipid bilayer solutions, required amounts of Laurdan/chloroform and lipid/chloroform for a final concentration of 5 μM of Laurdan and 2 mM of lipid were dried, water added, and the mixture stirred for 20 hours with a magnetic stirrer.

2.3. Fluorescence Measurements: Emission was excited at 340 nm for non-polar and 360 nm for all other solvents. Spectra were recorded with a Fluouromax-4 Spectroflourometer (Horiba Scientific) from 345 or 365 to 650 nm, at a step size of 0.5 as well as 1 nm and corrected for dark counts. Slit widths were 1 nm. Sample temperatures, measured by a thermocouple, ranged from 5 to 85 °C and maintained by a thermostated water bath.

2.4. Spectral Fitting: Spectra were fit to eq. 2, obtained from rewriting eq. 1 to change from the parameter a to linewidth $w = (k_{max} - k_{min})$,

$$\begin{cases} I(k) = I_m exp\left[-\frac{ln\,2}{ln^2(\rho)} ln^2\left(\frac{k_m+\frac{w\rho}{\rho^2-1}-k}{\frac{w\rho}{\rho^2-1}}\right)\right] & if\ k < k_m + \frac{w\rho}{\rho^2-1} \\ I(k) = 0 & if\ k \geq k_m + \frac{w\rho}{\rho^2-1} \end{cases} \quad (2)$$

Fits were performed by a Trust Region Reflective algorithm in MATLAB. It is an improvement over the Levenberg-Marquardt method. The measured wavelength spectra were first converted to wavenumber spectra by a Jacobian transformation and then fitted to one or more log-normal distributions in the form of eq. 2 [2,6]. The number of peaks fitted depends on the number of elementary emissions. SH of the spectral data were computed first. The spectra were fit to the number of peaks resolved in the SH spectra.

The SH signal E is a convolution of the modulation response function R and the fluorescence intensity I:

$$E = R * I \quad (3)$$

In analogy to field modulation used in ESR spectroscopy, the wavelength in the fluorescence spectra is modulated computationally with a sinusoidal signal of angular frequency ω_m and amplitude B_m. The modulation response function R is:

$$R = -\sum_{n=-\infty}^{\infty} \gamma J_n(\beta)(J_{n-2}(\beta) + J_{n+2}(\beta)) \quad (4)$$

where $J_n(\beta)$ is the Bessel function of order n, $\beta = \gamma B_m/\omega_m$ is the unitless index of modulation, and the gyromagnetic ratio, γ, is $1.76* 10^7$ $(sG)^{-1}$ [7,5].

The best fit was determined as the one with the flattest residuals of the fit to the spectra and of the SH of fit and SH of data and the best R^2. The SH residuals in particular aid in the decision of the best fit. Confidence intervals (95 %, or 2 x standard deviation) of the fitted parameters were obtained and are reported. Areas of the individual lines, representing their contributions to the total emission, were calculated from the fit parameters using the equation for the area of a log-normal distribution [8];

$$A = I_m w \left[\sqrt{2\pi}\ \frac{\rho}{\rho^2-1}\ c \exp\left(\frac{c^2}{2}\right)\right], \quad (5)$$

with $c = \frac{ln\rho}{\sqrt{2\ ln2}}$

The half-maximal positions were calculated using

$$k_{\max} = k_m + w\frac{1}{\rho+1} \quad (6)$$

$$k_{\min} = k_m - w\frac{\rho}{\rho+1} \quad (7)$$

Standard deviations in areas, k_{max}, k_{min} due to errors propagated from those in k_m, ρ, w, and I_m were calculated using error propagation formulae [9].

3.0. Results:

3.1. Homogenous Solvents: Fluorescence emission and the computed SH spectra of Laurdan in one example of each of non-polar, aprotic polar, and protic polar solvents are shown in Fig. 1 a-f together with the fits and residuals. The SH spectra of Laurdan in non-polar octane and in polar protic octanol exhibit the presence of two peaks. In acetone there is no evidence for a second emission. Spectra from aprotic polar solvents fitted best to a single line, and those from protic polar and non-polar were described better by two lines For purposes of identification, as is customary in Laurdan spectroscopy, the higher wavenumber peak is referred to as blue and the lower as red, in cases where there are two emission lines.

Clearly visible bumps are not always observed in SH as in octanol and octane (Fig. 1b and f). Spectra of Laurdan in butanol is an example. However, single line fits in such cases yielded poorer residuals than two-line fits as illustrated in the comparison in Fig. 2 a-d. Should emission characteristics be classified according to solvent polarity, then butanol exhibits behavior in agreement with its class of solvents. Tables 1- 3 in the supplemental information (SI) file list the best fit parameter values and their confidence intervals for homogeneous solvents.

3.2. Phospholipid Bilayers: Figures 3 a-d present emission and SH spectra in DSPC in gel (15 °C) and liquid (59 °C) phases together with fits and residuals. A second emission line, not visible in the emission spectra, is indicated in the SH spectra at 15 °C owing to the higher resolution of SH. Accordingly, the gel phase spectra were fit to two emission lines. The strong line, characteristic of gel phase bilayers, is at 445 nm. The position of the weak line is at 432 nm. Existence of this weak line has not been reported in lipid bilayer gel phases, because it is not distinguishable without the advantage of SH spectra. A comparison of fitting the bilayer gel spectra to one and two lines is made available in the SI. Residuals are flatter for the two line fits.

The nature of Laurdan spectra in bilayers has been well-studied [3,10-16]. Laurdan emissive state in bilayer gel phases is modeled to be a charge transfer unrelaxed state (CT_{ur}) state that emits a single strong blue line around 440 nm [3,11]. Present SH spectra and fits show evidence for two emissive states even in the gel phase.

Figures 3 c and d present the spectra, SH, fits and residuals in the DSPC bilayer liquid phase at 59 °C. Two well-resolved peaks are observed in the SH as reported for bilayer liquid phases. Fit to the spectrum yields peak positions of 429 nm and 484 nm. The longer wavelength (red) emission in the liquid domains is from the solvent (water) relaxed excited state (CT_r) and the shorter blue wavelength line is from the gel domains which persist even after the transition at 54 °C [3].

3.3. *Phospholipid Bilayer Gel to Liquid transition:* Laurdan emission spectra at various temperatures shown in Fig. 4 illustrate the well-documented coexistence of gel and liquid domains and the red-shift of Laurdan emission that accompany the gel to liquid transition. The red-shift is parametrized by the generalized polarization (GP) [13,17,14],

$$GP = \frac{I_{435}-I_{480}}{I_{435}+I_{480}}, \quad (8)$$

where I is the intensity at the wavelength in the subscript. GP falls steeply with temperature, as in Fig. 5a, signifying the phase transition at 54 °C for DSPC. Included in Fig. 5a are wavelengths of the peak positions. The areas of the individual lines calculated using eq. 5 and the total area vary with temperature according to Fig. 5b. The longer wavelength line at 445 nm, contributing close to 92 % of the emission, is the dominant peak in the bilayer gel phase. It continues as the dominant line and its peak wavelength position continuously and rapidly increases with temperature in the transition region. The continuous red shift in the peak position suggests that the emission state is in varying degrees of relaxation.

The total area decreases in the transition region. The total area at 15 °C is set to unity. The areas at higher temperatures are expressed as fractions of the area at 15 °C. The area of the red line decreases in the pre-transition region followed by an increase post-transition. The red-shift is as expected. Curiously the area of the blue line increases from 0.07 at 15 °C to 0.24 at 54 °C followed by a sharp decline, but continues thereafter to decrease gradually to a value of 0.12 at 59 °C. The position of the blue line shifts only a few nm. This shift, however is significant and together with the contradictory behavior of its area increase and the trajectories of the red and blue peak positions vs temperature (Fig. 5a) provides context to the model presented in Section 4.0.

Similar results were obtained for DPPC. Table 4 gives the fit results for DPPC and DSPC.

3.4. Additional Notes on Fitting and Constraints: The half maximal positions k_{min} and k_{max} of the single lines in aprotic polar and the red lines in the nonpolar and protic polar solvents and in lipid bilayers are examined as a function of peak positions k_m in Fig. 6 a. Linear regression analyses on the data of only the single line in aprotic polar solvents yield;

$$k_{max} = 15906 + 0.989 \, x \, k_m \quad (9)$$

$$k_{min} = -387 + 0.998 \, x \, k_m \quad (10)$$

A linear variation is in agreement with observations for other fluorescent probes and for Laurdan [1,2]. These equations have the appeal of constraints to reduce the number of fit parameters when fitting multiple line spectra where observed.

However, use of these linear relations to constraint fits to two line spectra of nonpolar and protic polar solvents and lipid bilayers did not yield fits better than with unconstrained parameters. The k_{min} and k_{max} points for the red line of all other solvents derived from unconstrained fits fall

close to the line for aprotic polar solvents. But constraining them to be exactly on the line does not seem a better option. In some cases constrained fits could be considered reasonable had the results of the option of floating all parameters were not available. An example of constrained and unconstrained fits is given in the SI. Residuals are better for the unconstrained fit, especially in the SH.

k_{min} and k_{max} of the blue lines of nonpolar and protic polar solvents and lipid bilayers also show a near linear variation with k_m as in Fig. 6b. The slopes, 0.77 of k_{max} and 1.28 of k_{min} are different from each other and from the slopes of the red line parameters (eq. 9 and 10). The constraint equations obtained from the aprotic polar solvent data cannot reasonably be expected to apply to this line. Nevertheless, a comparison of fits to DSPC spectra and SH at 59 °C without and with both lines constrained by eq. 9 and 10 is presented in the SI. Residuals, particularly in the blue part of the SH, are improved in the unconstrained fit.

4.0. Discussion:

The model of Laurdan emission in bilayers and low viscosity homogenous solvents, like those in the present work, proposes two types of emissive states; unrelaxed and relaxed charge transfer states (CT_{ur} and CT_r) [18,15]. Another emissive state of Laurdan, the locally excited state (LE) has been observed only in highly viscous non-polar solvents and in frozen ethanol [11].

4.1. Lipid Bilayers: The dominant line at 445 nm with about 92 % of emission has hitherto been supposed to be the only peak in the gel phase and modeled to be a CT_{ur} excited state emission. Existence of the weaker line elicited by SH and the temperature dependence of the peak positions and areas (Fig. 5 a and b) compel an adjustment to this assignment. The continuous red-shift in the peak position of the dominant line suggests that the emission is from a state that becomes increasingly relaxed with temperature. Increase in interfacial water concentration and water mobility and reduced lipid packing that accompany temperature and phase change promote dipolar relaxation of the excited state and thus an increasingly lower energy relaxed emissive state. The weak blue line on the other hand, because it shifts minimally in the transition region, has the character of emission from an unrelaxed state whose environment does not change as significantly as that of the red line excited state.

The dominance of the red line suggests that the bilayer has a larger extent of less packed lipid regions and thereby a larger fraction of Laurdan. The decrease in the area of the red line is attributed to quenching of fluorescence by oxygen diffusing into domains with temperature and phase induced decreased lipid packing [19]. Laurdan is not quenched in the tighter packed gel phase, and the areas remain constant [19]. The increase in the area of the blue line, as the temperature approaches transition, appears anomalous because increased quenching in one domain modulates quenching in the other domain as well [20]. Quenching by oxygen should decrease areas of both lines. As the entire structure experiences reduced lipid packing, the blue line emission is expected to decrease and red-shift in a similar manner to the red line if they are both

from the same region. The different trajectories of the red and blue lines indicate that they originate from Laurdan in two differently packed regions, prompting the conclusion that even the gel phase is inhomogeneous. Laurdan from the tighter packed regions emits the blue line, and the red line is from the less packed region. As temperature increases, the structure becomes increasingly relaxed. Both lines red-shift in the pre-transition region (51 °C < T < 54 °C). The blue line red shifts only by 3 nm and the red line by 13 nm. After the transition, the blue line shifts down by 6 nm and the red line continues to red shift to 484 nm at 59 °C.

Vesicles undergo changes in shape as they transform from gel to liquid phase [21,22]. Gel and liquid phases coexist at about the transition temperature. Gel phases were observed to exist as a flat bilayer whereas liquid phases formed high curvature domains. Laurdan distributes between gel and liquid phases, but it prefers flat regions [18]. Results in Fig. 5 show that there are are two domains of different lipid packing before, through, and after transition. As the looser packed domains increase in curvature, Laurdan shifts to tighter packed domains of lower curvature. This could account for the increase in the area of the blue line. After the transition, the gel domains experience increased stress and lipid packing due to inhomogeneous curvature distribution and the blue peak shifts down in wavelength due to the decreased polarity of that region[12]. The contribution of the blue line decreases post-transition because of the increase in the extent of the liquid domains, and Laurdan distribution shifts toward liquid domains. The small shift of the blue line from 435 nm at 54 °C to 429 nm is consistent with increased lipid packing in the low curvature gel domains and stresses induced by inhomogeneity in curvature.

4.2. Homogeneous Solvents: Solvent relaxation time scales are three to four orders of magnitude faster than the fluorescence lifetimes in low viscosity homogeneous solvents at temperatures higher than about 200 K[23]. Steady state emissions under these conditions are therefore from solvent relaxed states. In all of the homogenous solvents and lipid bilayers, the red line is the dominant line. It appears from Fig. 6 that red lines of all solvents form a class that share some common feature as do the blue lines. Experiments and computational calculations have shown that the higher and lower wavenumber emissions observed in hexane are from nonplanar and planar conformations of Laurdan respectively [24]. In protic polar solvents, Laurdan in planar conformation was shown to interact with the solvent molecule only through its carbonyl oxygen [24]. Laurdan's ability to accept hydrogen bonds was suggested to be responsible for a red shift that increased with the proportion of protic polar component in mixed protic and aprotic polar solvents [4]. The red line in protic polar solvents might therefore be from a planar conformation. The nonplanar conformation, responsible for the blue line, interacts through carbon atoms as well as suggested by other authors [24]. Alcohols are known to exist in nanostructured polar and nonpolar domains; exhibiting nonpolar and polar character that can give rise to different interactions with Laurdan, and thus to multiline spectra [25]. Dipolar relaxation dominates in aprotic polar solvents. When continuing with the same rationale, planar conformation for Laurdan is suggested.

Laurdan in bilayers adopts a planar conformation and solvent dipolar interaction is responsible for the red line in the gel and liquid phases [26]. The blue line in bilayers may conceivably be an emission from a nonplanar configuration because its k_{max} and k_{min} share the same linear variation with k_m (Fig. 6b) as those of the blue lines of nonpolar and protic polar solvents.

5.0. Summary and Conclusions:

Complementary fitting and analyses of Laurdan fluorescence emission and second harmonic spectra in homogeneous solvents and lipid bilayers were conducted. Spectra were fit to log-normal distributions. Higher resolution afforded in the SH showed two emissions in protic polar and nonpolar solvents and in both of bilayer gel and liquid phases and a single line in aprotic polar solvents. The shorter wavelength 432 – 434 nm line in the gel phase, distinguishable in the SH, is the weaker one of the two. This line shifts minimally compared to the stronger red line as the bilayer transitions from gel to liquid. While GP captures the red-shift, the areas and peak positions of the individual lines express the nature and evolution of inhomogenous lipid packing, The blue line is identified as a CT_{ur} emission from Laurdan in tighter packed lipid regions and the dominant 445 - 448 nm line in the gel phase shifting to 484 nm in the liquid phase as the CT_r line that is in varying stages of relaxation beginning as unrelaxed at low temperatures in the gel phase. Thus the presence of two lines indicates inhomogeneous lipid packing even in the gel phase. Preference for flat low curvature domains over higher curvature domains is an unexploited property of Laurdan. Application of this property to vesicles changing in shape during the transition due to coexisting high and low curvature rationalizes the unexpected increase in the area of the blue line during the transition.

References

1. Burstein EA, Emelyanenko VI (1996) Log-Normal Description of Fluorescence Spectra of Organic Fluorophores. Photochemistry and Photobiology 64 (2):316-320. doi:10.1111/j.1751-1097.1996.tb02464.x

2. Bacalum M, Zorila B, Radu M (2013) Fluorescence spectra decomposition by asymmetric functions: Laurdan spectrum revisited. Analytical Biochemistry 440:123-129

3. Parasassi T, Krasnowska EK, Bagatolli L, Gratton E (1998) Laurdan and Prodan as Polarity-Sensitive Fluorescent Membrane Probes. Journal of Fluorescence 8 (4):365-373. doi:10.1023/A:1020528716621

4. Bacalum M, Zorila B, Radu M, Popescu A (2013) Laurdan solvatochromism: Influence of solvent polarity and hydrogen bonds. Optoelectronics and Advanced Materials: Rapid Communications 7:456-460

5. Bluzas GL (1995) Study of modulation effects on ESR spectra.

6. Mooney J, Kambhampati P (2013) Get the Basics Right: Jacobian Conversion of Wavelength and Energy Scales for Quantitative Analysis of Emission Spectra. The Journal of Physical Chemistry Letters 4 (19):3316-3318. doi:10.1021/jz401508t

7. Poole CPJ (1983) Electron Spin Resonance: A Comprehensive Treatise on Experimental Technique. 2nd edn. Wiley, New York

8. Siano DB, Metzler DE (1969) Band Shapes of the Electronic Spectra of Complex Molecules. The Journal of Chemical Physics 51 (5):1856-1861. doi:10.1063/1.1672270

9. Ku HH (1966) Notes on the use of Propagation of error Formulas. JOURNAL OF RESEARCH of the National Bureau of Standards-C Engineering and Instrumentation 70C (4):263-273

10. Bagatolli LA, Parasassi T, Fidello GD, Gratton E (1999) A Model for the Interaction of 6-Lauroyl-2-(N,N-dimethylamino)naphthalene with Lipid Environments: Implications for Spectral Properties. Photochemistry and Photobiology 70(4):557-564

11. Viard M, Gallay J, Vincent M, Meyer O, Robert B, Paternostre M (1997) Laurdan solvatochromism: solvent dielectric relaxation and intramolecular excited-state reaction. Biophys J 73 (4):2221-2234. doi:10.1016/s0006-3495(97)78253-5

12. Bagatolli LA (2006) To see or not to see: Lateral organization of biological membranes and fluorescence microscopy. Biochimica et Biophysica Acta (BBA) - Biomembranes 1758 (10):1541-1556. doi:https://doi.org/10.1016/j.bbamem.2006.05.019

13. Harris FM, Best KB, Bell JD (2002) Use of laurdan fluorescence intensity and polarization to distinguish between changes in membrane fluidity and phospholipid order. Biochimica et Biophysica Acta (BBA) - Biomembranes 1565 (1):123-128. doi:https://doi.org/10.1016/S0005-2736(02)00514-X

14. Parasassi T, Stasio G, Ravagnan G, Rusch RM, Gratton E (1991) Quantitation of lipid phases in phospholipid vesicles by the generalized polarization of Laurdan fluorescence. Biophys J 60:179-189

15. Vincent M, de Foresta B, Gallay J (2005) Nanosecond Dynamics of a Mimicked Membrane-Water Interface Observed by Time-Resolved Stokes Shift of LAURDAN. Biophysical Journal 88 (6):4337-4350. doi:https://doi.org/10.1529/biophysj.104.057497

16. Parasassi T, De Stasio G, d'Ubaldo A, Gratton E (1990) Phase fluctuation in phospholipid membranes revealed by Laurdan fluorescence. Biophysical Journal 57 (6):1179-1186. doi:https://doi.org/10.1016/S0006-3495(90)82637-0

17. Merlo S, Yager P (1990) Optical method for monitoring the concentration of general anesthetics and other small organic molecules. An example of phase transition sensing. Analytical Chemistry 62 (24):2728-2735. doi:10.1021/ac00223a015

18. Viard M, Gallay J, Vincent M, Paternostre M (2001) Origin of laurdan sensitivity to the vesicle-to-micelle transition of phospholipid-octylglucoside system: a time-resolved fluorescence study. Biophys J 80 (1):347-359. doi:10.1016/s0006-3495(01)76019-5

19. Parasassi T, Gratton E (1992) Packing of phospholipid vesicles studied by oxygen quenching of Laurdan fluorescence. Journal of Fluorescence 2 (3):167-174. doi:10.1007/bf00866931

20. Parasassi T, Ravagnan G, Rusch RM, Gratton E (1993) Modulation and dynamics of phase properties in phospholipid mixtures detected by laurdan fluorescence*. Photochemistry and Photobiology 57 (3):403-410. doi:10.1111/j.1751-1097.1993.tb02309.x

21. Bagatolli LA, Gratton E (2001) Direct Observation of Lipid Domains in Free-Standing Bilayers Using Two-Photon Excitation Fluorescence Microscopy. Journal of Fluorescence 11 (3):141-160. doi:10.1023/a:1012228631693

22. Parasassi T, Gratton E, Yu WM, Wilson P, Levi M (1997) Two-photon fluorescence microscopy of laurdan generalized polarization domains in model and natural membranes. Biophysical Journal 72 (6):2413-2429. doi:https://doi.org/10.1016/S0006-3495(97)78887-8

23. Fourkas JT, Berg M (1993) Temperature-dependent ultrafast solvation dynamics in a completely nonpolar system. The Journal of Chemical Physics 98 (10):7773-7785. doi:10.1063/1.464585

24. Morozova Y, Zharkova O, Balakina T, Artyukhov V, Korolev B (2011) Conformal transitions of the laurdan molecule in the absorption and fluorescence spectra. Russian Physics Journal 54:594-600. doi:10.1007/s11182-011-9657-5

25. Chen B, Siepmann JI (2006) Microscopic Structure and Solvation in Dry and Wet Octanol. The Journal of Physical Chemistry B 110 (8):3555-3563. doi:10.1021/jp0548164

26. Bagatolli LA, Parasassi T, Fidelio GD, Gratton E (1999) A Model for the Interaction of 6-Lauroyl-2-(N,N-dimethylamino)naphthalene with Lipid Environments: Implications for Spectral Properties. Photochemistry and Photobiology 70 (4):557-564. doi:10.1111/j.1751-1097.1999.tb08251.x

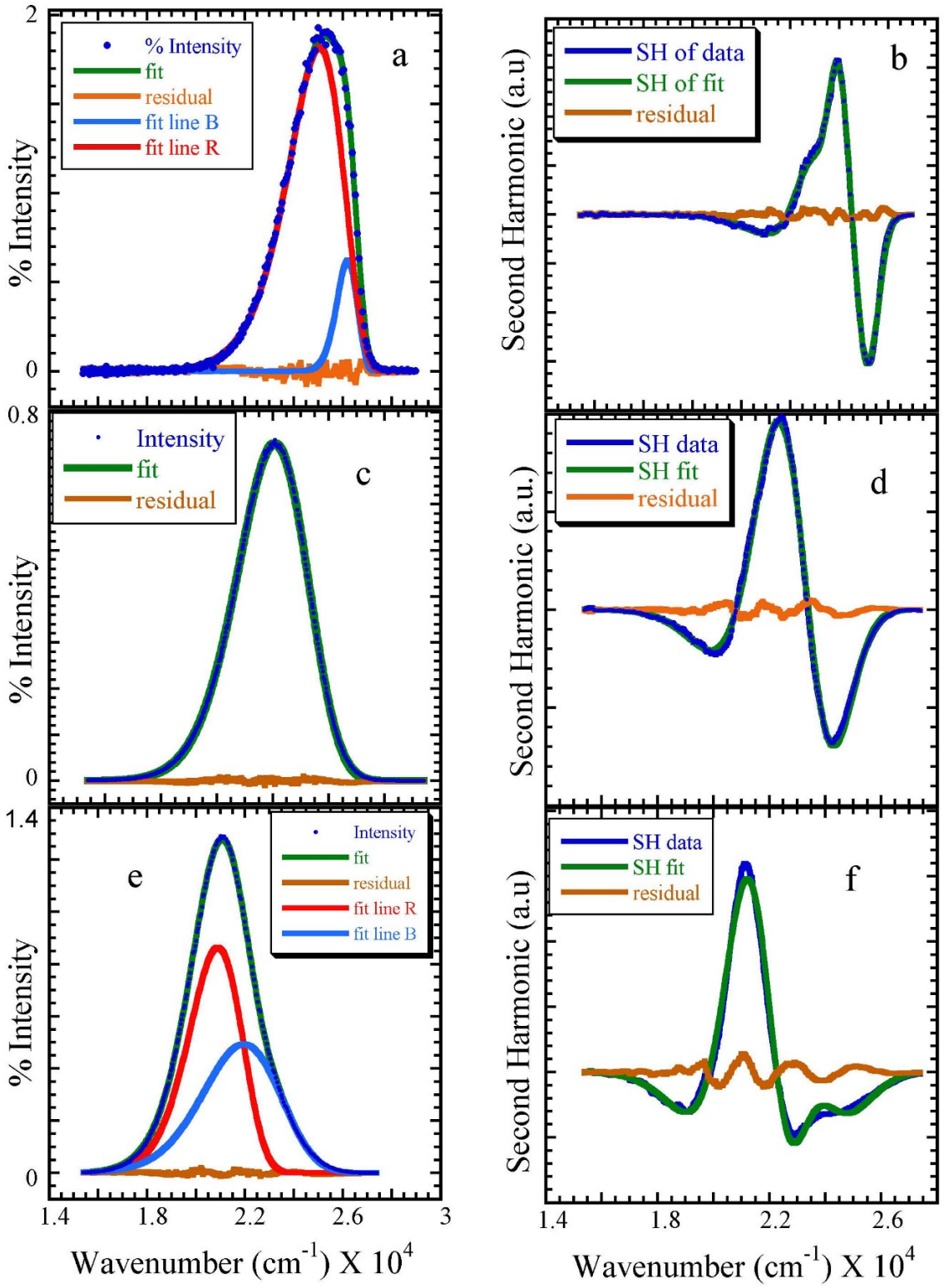

Figure 1: Laurdan emission (a, c, e) and SH (b, d, f) spectra, fits and residuals in one example each of: nonpolar octane (a, b); aprotic polar acetone (c, d); protic polar octanol (e,f) at 5°C. Excitation wavelength was 340 nm for octane and 360 nm for acetone and octanol.

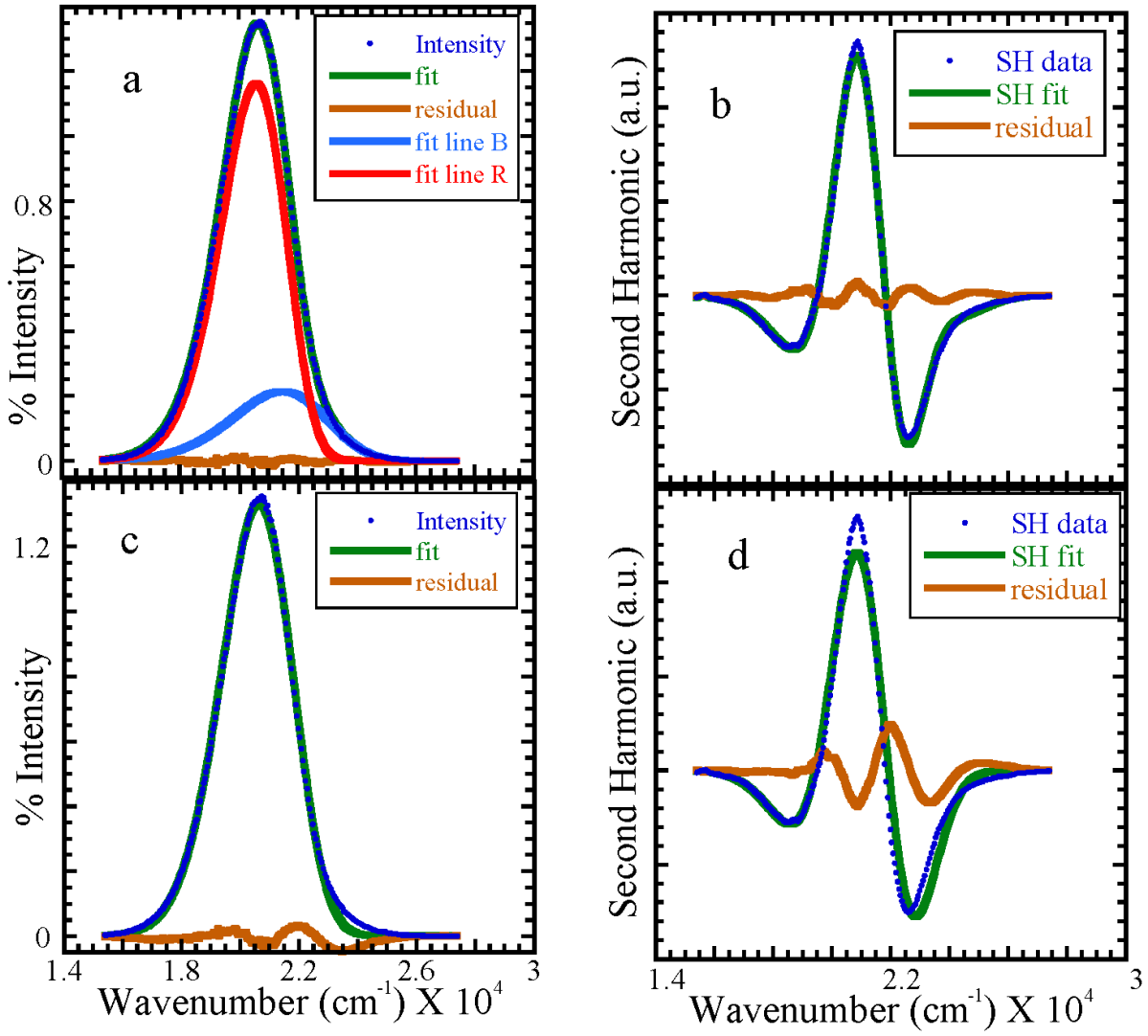

Figure 2: Comparison of two line (a,b) and one line (c,d) fits of Laurdan emission (a, c) and SH (b, d) spectra and residuals in butanol at 5°C.

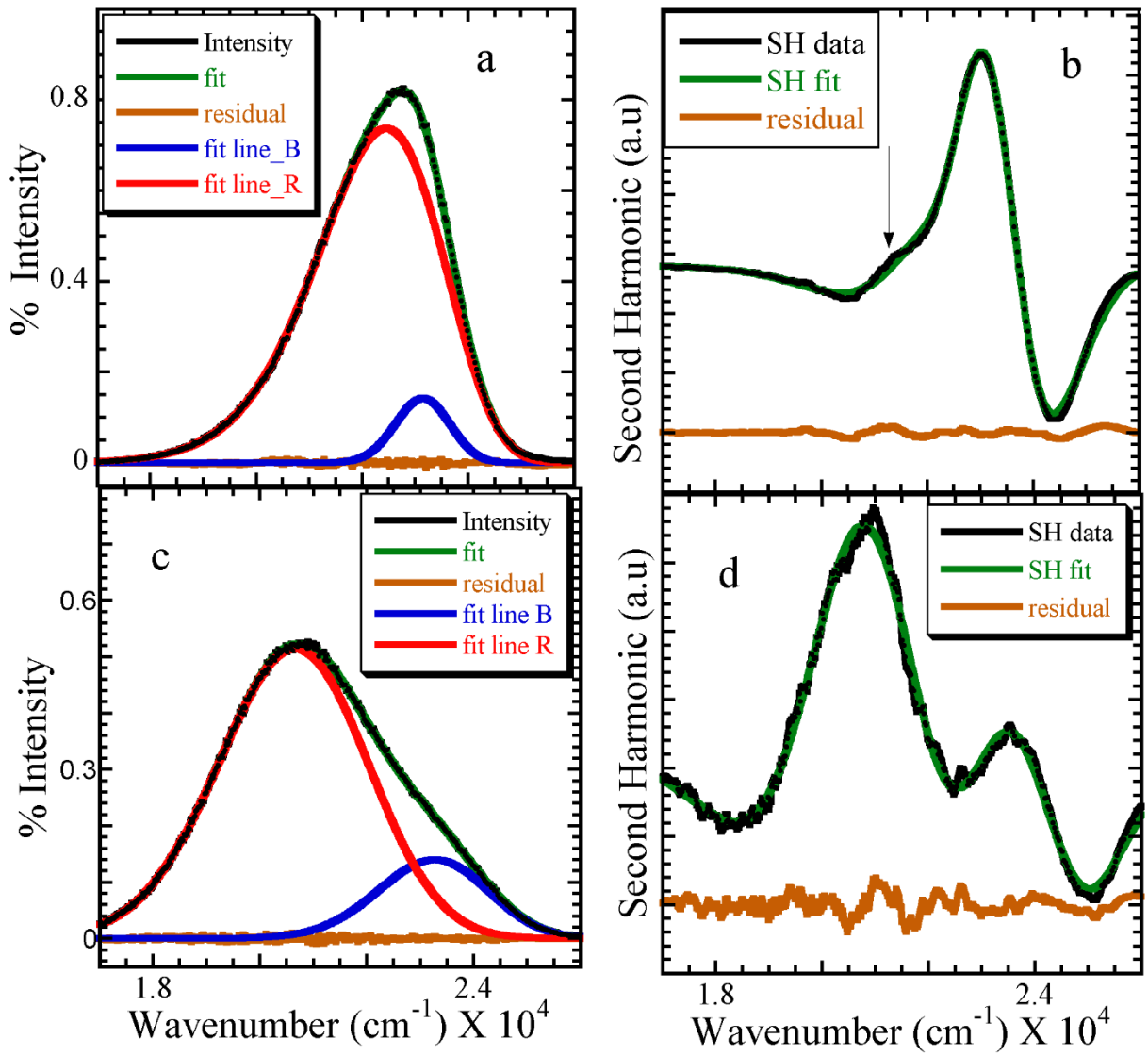

Figure 3: Laurdan emission (a, c) and SH (b, d) spectra, fits (solid line) and residuals in DSPC. Gel phase 15 °C (a, b). Liquid phase 59 °C (c, d). The arrow in Fig. 3b helps indicate existence of two peaks. Excitation wavelength was 360 nm.

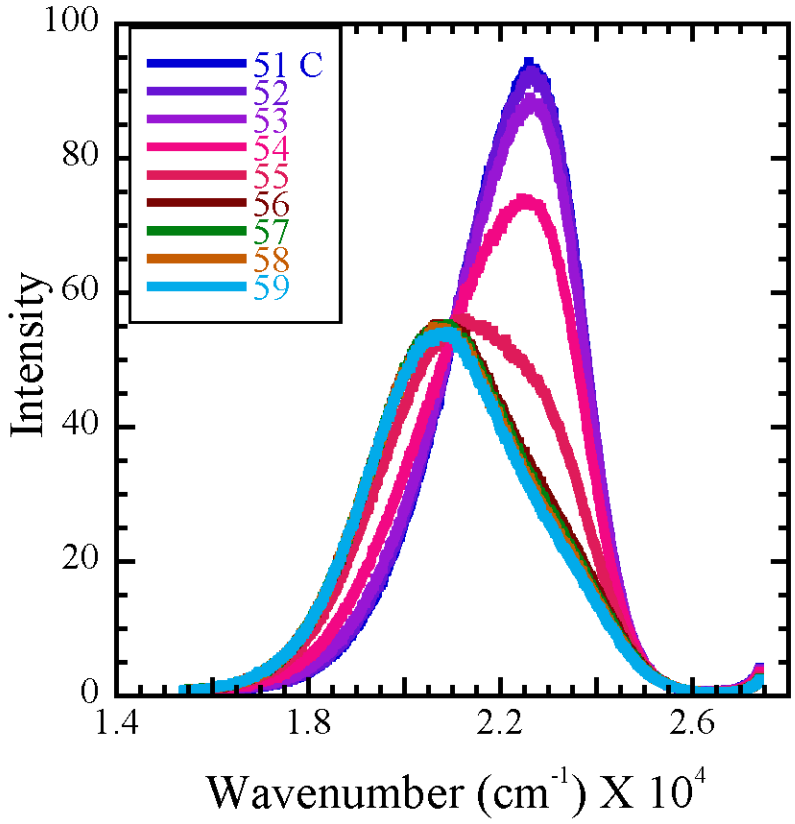

Figure 4: Laurdan emission spectra of DSPC at various temperatures in the transition region.

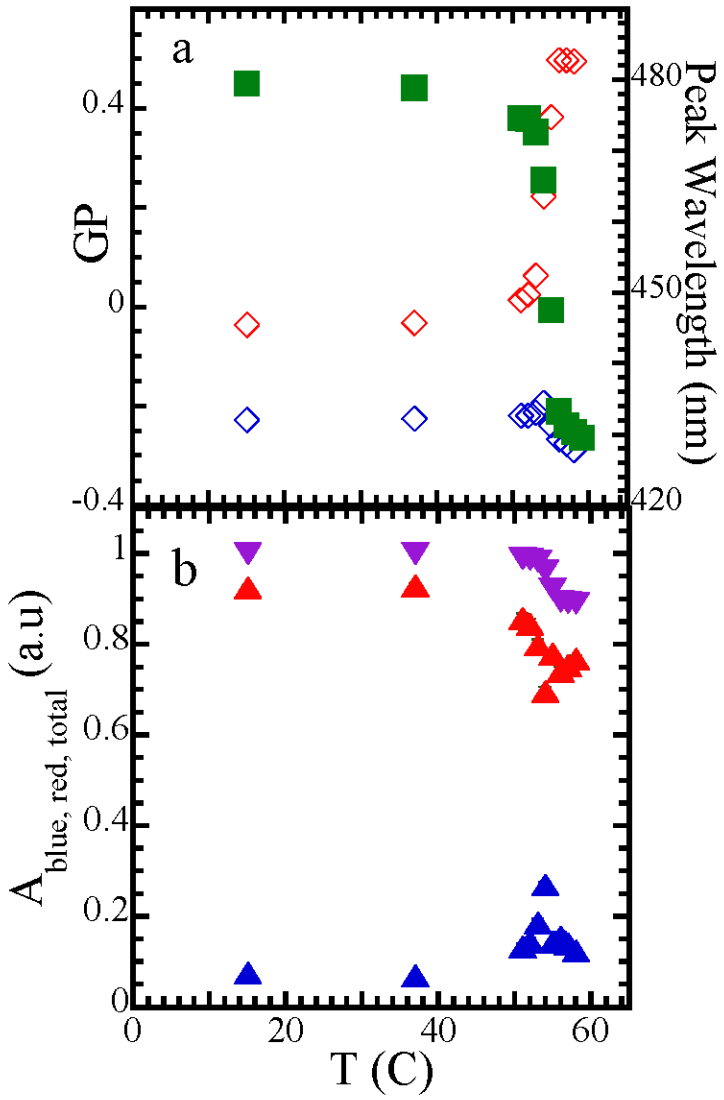

Figure 5: Spectral characteristics as a function of temperature in the gel-liquid transition region of DSPC. (a) GP (■ left side ordinate) and peak wavelengths (right side ordinate) of the red (◇) and blue (◇) lines; (b) areas of the red (▲) and blue (▲) lines and the total area (▼). Error bars are standard deviations from the fits and are about the size of the symbols

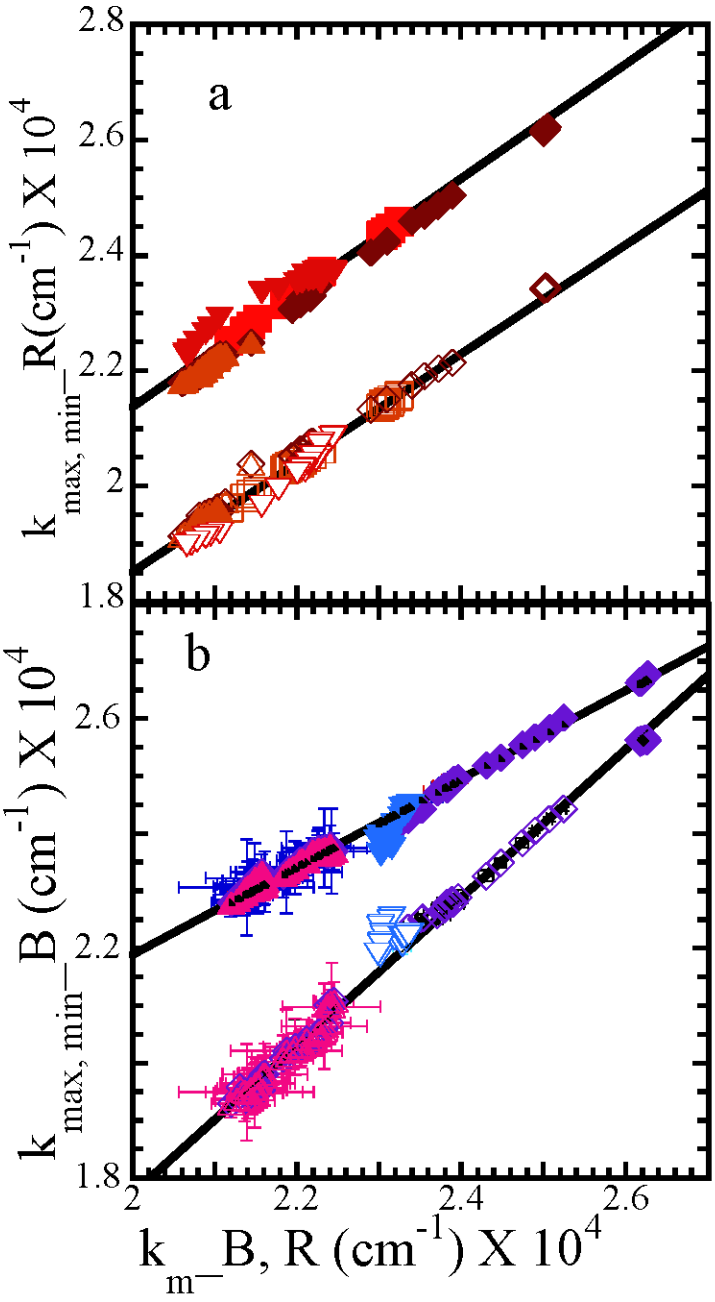

Figure 6: Half maximal positions k_{max}, k_{min} vs peak position, k_m of (a) red lines and (b) blue lines at all measured temperatures for all homogenous solvents and bilayers. Solid symbols are for k_{max} and open symbols for k_{min}. Nonpolar (♦, ◇), lipid bilayers (▼, ∇), aprotic polar (■, □□), protic polar (▲, Δ). Solid lines are linear fits to (a) data on aprotic polar solvents only, (b) all points.

Supplemental Information

Complementary Fluorescence Emission and Second Harmonic Spectra Improve Bilayer Characterization

Radha Ranganathan, Asher J. Burkin, and Miroslav Peric

Department of Physics, California State University Northridge, CA 91311, U.S.A.

Corresponding Author: Radha Ranganathan: radha.ranganathan@csun.edu

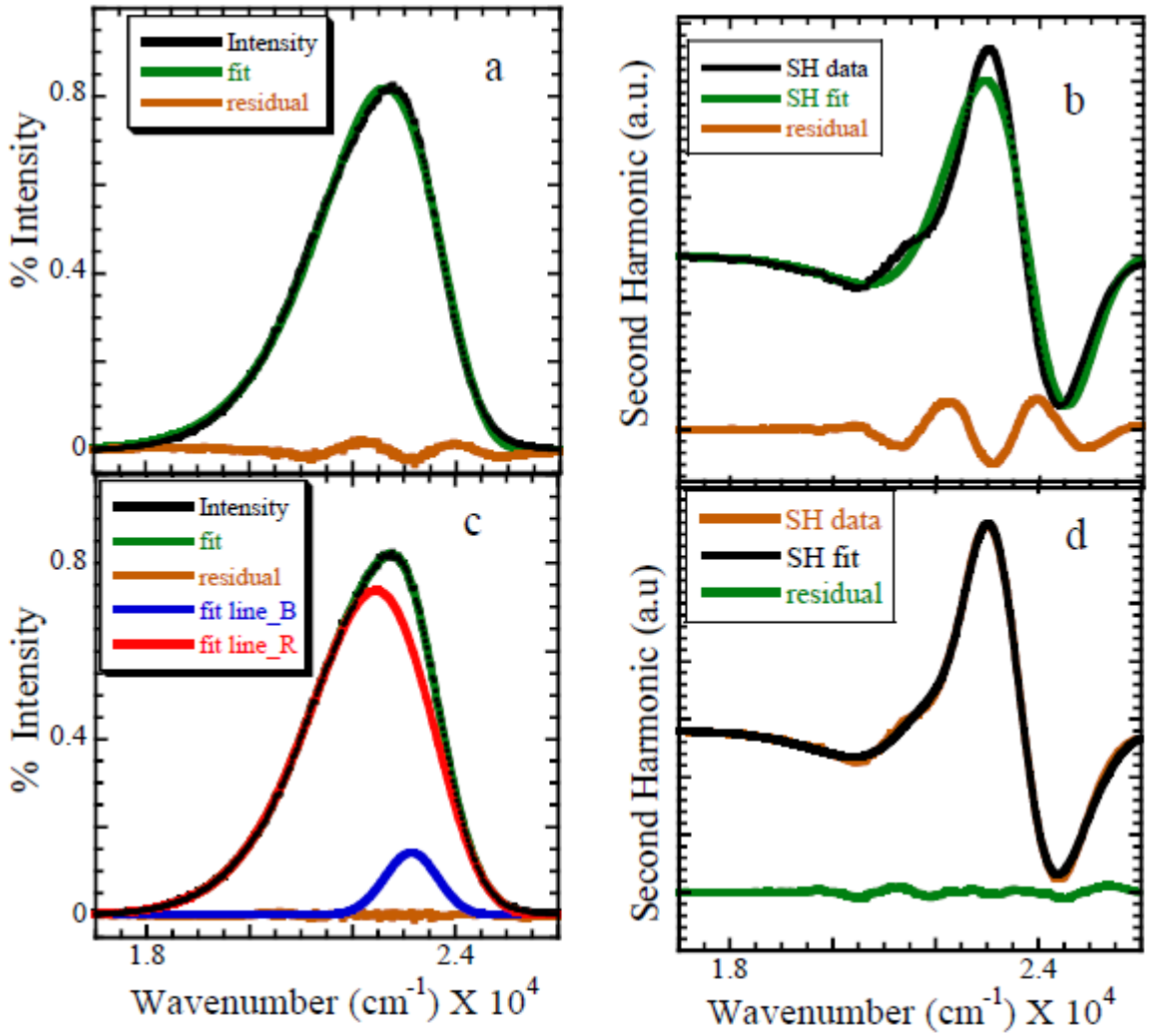

Figure S1: Comparison of fits to spectra in DSPC at 15 °C with one (a,b) and two (c,d) log-normal functions.

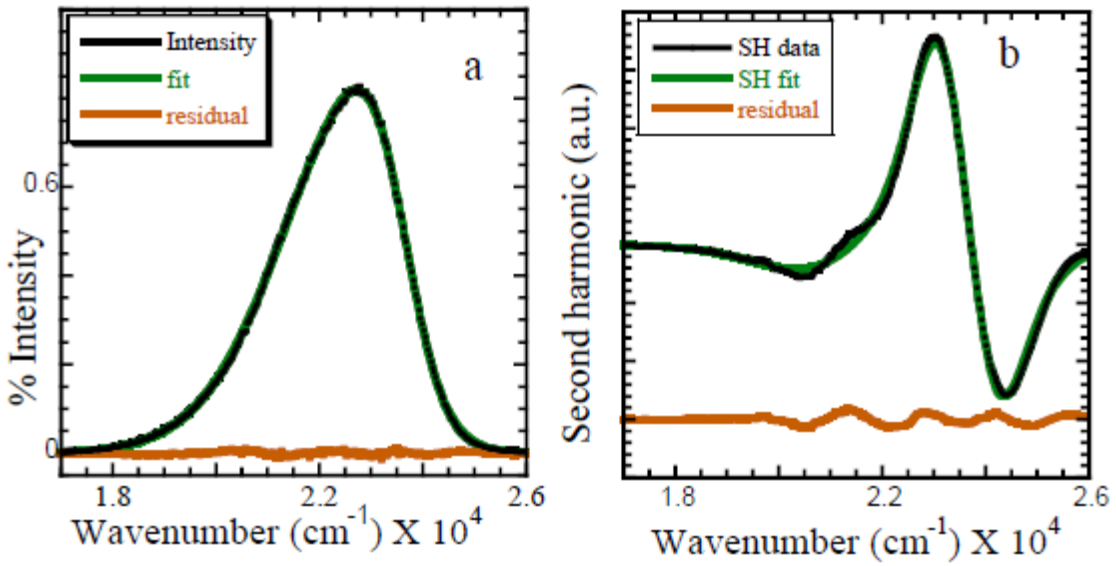

Figure S2: Constrained fit to the spectrum in DSPC at 15 °C. The dominant line parameters were constrained by eq. 9 and 10, which leaves two parameters I_m and k_m for this line and four for the blue line. The fits and residuals are to be viewed in comparison with Fig. S1 c and d.

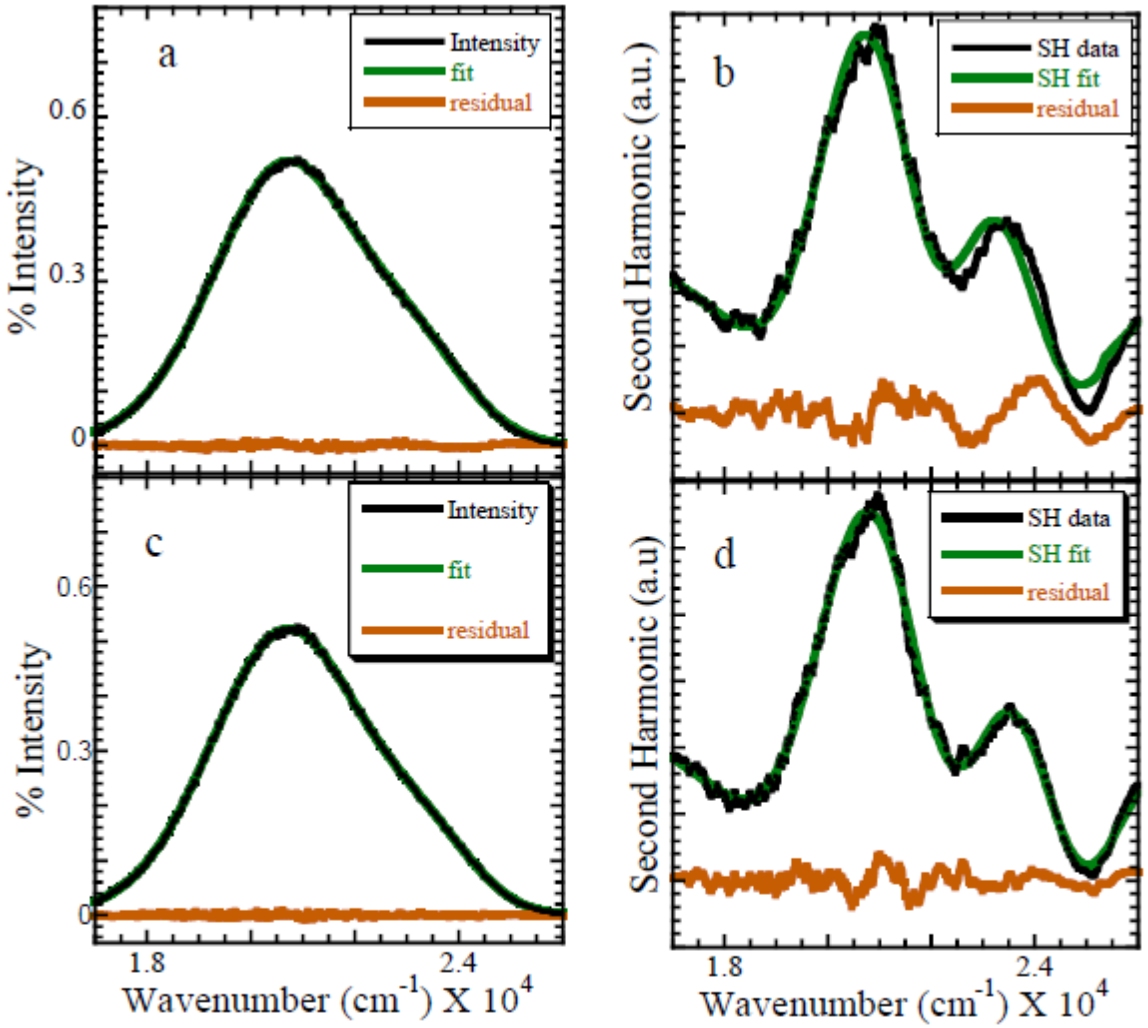

Figure S3: Comparison of fit to DSPC spectra at 59 °C (a, b) with both lines constrained by eq. 9 and 10 and (c, d) unconstrained.

Table 1: Parameter values of fits in aprotic polar solvents and their 95 % confidence intervals

T (°C)	*λ_{exc} (nm)*	*a*	*k_m (cm^{-1})*	*ρ*	*k_{max} (cm^{-1})*	*k_{min} (cm^{-1})*	*width (cm^{-1})*
Acetonitrile							
5	360	30060±66	21908±1.4	1.19±0.002	23229±14	20367±18	2862±24
25	360	30600 ±58	21977±1.2	1.18±0.001	23337±12	20408±16	2929±20
50	360	31008 ±64	22071±1.2	1.18±0.001	23447±12	20471±16	2976±20
			Acetone				
5	340	31484±128	22067±2.2	1.17±0.002	23447±25	20471±32	2975±41

15	340	31733±126	22125±2.1	1.17±0.002	23529±25	20513±31	3017±40
25	340	31965±135	22191±2.3	1.17±0.002	23613±26	20555±33	3058±42
45	340	32289±142	22302±2.3	1.17±0.003	23753±27	20661±34	3092±44
5	360	31477±112	22067±2.0	1.17±0.002	23447±22	20471±28	2976±36
15	360	31775±113	22123±1.9	1.17±0.002	23529±22	20513±28	3017±36
25	360	31963±119	22191±2.0	1.17±0.002	23613±23	20555±29	3058±37
45	360	32324±130	22300±2.1	1.16±0.002	23725±25	20661±31	3064±40
			Dimethylformamide				
5	340	29895±103	21869±2.3	1.19±0.003	23175±22	20325±29	2850±37
15	340	30150±109	21910±2.3	1.19±0.003	23229±23	20367±30	2862±38
25	340	30464±116	21950±2.3	1.18±0.003	23283±24	20387±31	2896±40
50	340	31308±130	22032±2.3	1.17±0.003	23419±26	20450±33	2969±42
5	360	29872±94	21873±2.1	1.19±0.002	23202±21	20325±27	2877±34
15	360	30191±104	21911±2.2	1.19±0.002	23229±22	20346±29	2883±36
25	360	30572±107	21950±2.1	1.18±0.002	23310±22	20387±29	2923±37
50	360	31273±118	22036±2.1	1.17±0.002	23419±24	20450±30	2969±38
			Dimethylsulfoxide				
5	340	31182±184	21171±2.7	1.15±0.003	22523±33	19627±42	2895±53
15	340	31011±160	21353±2.5	1.16±0.003	22701±30	19802±38	2899±48
25	340	31230±163	21439±2.5	1.16±0.003	22805±31	19881±38	2924±49
50	340	32160±184	21519±2.5	1.15±0.003	22910±33	19940±40	2969±52
5	360	31068±164	21187±2.5	1.16±0.003	22548±30	19646±38	2902±48
15	360	30958±148	21370±2.4	1.16±0.003	22727±28	19822±35	2906±45
25	360	31134±161	21440±2.6	1.16±0.003	22805±31	19881±38	2924±49
50	360	31919±169	21523±2.4	1.15±0.003	22936±31	19920±38	3016±49
			Ethylacetate				
5	340	30132±84	23023±2.6	1.23±0.003	24390±21	21368±29	3023±36
15	340	30176±88	23076±2.7	1.23±0.003	24450±22	21413±31	3037±38
25	340	30267±91	23133±3.0	1.23±0.003	24510±25	21459±34	3051±42
50	340	30574±101	23244±3.0	1.23±0.003	24631±25	21575±28	3056±43
5	360	30078±80	23009±2.5	1.23±0.003	24361±20	21368±28	2993±35
15	360	30082±79	23068±2.5	1.24±0.003	24420±20	21413±28	3007±34
25	360	30240±81	23123±2.5	1.24±0.003	24480±21	21459±28	3021±35
50	360	30613±90	23233±2.7	1.23±0.003	24631±25	21552±31	3079±38
			Propylene Carbonate				
5	340	30038±76	21846±1.6	1.19±0.002	23175±16	20284±21	2891±27
15	340	30392±82	2187±1.7	1.18±0.002	23202±17	20305±22	2897±28
25	340	30764±87	21900±1.6	1.18±0.002	23256±18	20325±23	2931±29
46	340	31444±98	21952±1.7	1.17±0.002	23337±19	20367±24	2971±31

66	340	32202±107	21996±1.6	1.16±0.002	23419±20	20387±25	3032±32
87	340	32899±116	22040±1.6	1.15±0.002	23474±21	20408±26	3066±33
5	360	30123±94	21843±2.2	1.19±0.002	23175±26	20284±26	2891±33
15	360	30465±100	21868±2.2	1.18±0.002	23202±21	20305±27	2897±34
25	360	30805±101	21898±2.2	1.18±0.002	23256±21	20325±26	2931±34
46	360	31540±112	21950±2.2	1.17±0.002	23337±22	20367±27	2971±35
66	360	32197±121	21996±2.2	1.16±0.002	23419±23	20387±28	3032±36
87	360	32966±130	22039±2.2	1.15±0.002	23474±23	20408±29	3066±37
			Tetrahydrofuran				
5	340	29211±65	23057±2.5	1.26±0.003	24361±104	21459±25	2901±31
15	340	29390±66	23104±2.5	1.26±0.003	24420±104	21482±26	2938±31
25	340	29555±71	23154±2.6	1.26±0.003	24480±109	21529±27	2951±34
50	340	29927±70	23255±2.4	1.25±0.003	24600±102	21598±26	3002±32
5	360	29210±61	23056±2.3	1.26±0.003	24361±99	21436±24	2924±29
15	360	29361±63	23103±2.4	1.26±0.003	24420±100	21482±25	2938±30
25	360	29562±63	23152±2.3	1.26±0.003	24480±97	21529±24	2951±30
50	360	29895±61	23251±2.1	1.25±0.003	24600±89	21598±23	3002±28

Table 2: Parameter values of fits to spectra in nonpolar solvents and their 95 % confidence intervals. Excitation wavelength for octane and hexane was 340 nm and 360 nm for all others.

T (°C)	k_{mB} (cm^{-1})	width_B (cm^{-1})	ρ_B	k_{mA} (cm^{-1})	width_A (cm^{-1})	ρ_A
Dioxane						
5	23791±103	2009±43	1.075±0.02	22141±94	2827±103	1.30±0.03
25	23818±142	2111±76	1.08±0.04	22110±131	2819±128	1.30±0.03
50	23921±129	2154±91	1.02±0.04	22194±106	2833±106	1.31±0.03
Chloroform						
5	23202±52	1882±43	1.11±0.01	21942v104	2545±99	1.26±0.03
25	23353±57	1879±41	1.11±0.02	22046±112	2526±110	1.26±0.03
50	23508±63	1905±46	1.11±0.02	22161±124	2521±125	1.27±0.03
Octane						
5	26181±14	1065±52	1.21±0.08	25011±32	2762±38	1.36±0.02
15	26173±15	1073±56	1.21±0.08	25006±33	2766±38	1.34±0.02
25	26220±18	1097±71	1.21±0.09	25017±44	2742±60	1.37±0.03
50	26240±24	1134±102	1.23±0.11	25002±67	2747±94	1.37±0.04
65	26240±24	1134±102	1.23±0.11	25002±67	2747±94	1.37±0.04
Tolune						
5	24298±87	1930±84	1.17±0.04	22901±129	2720±122	1.35±0.03

15	24474±69	1839±62	1.16±0.03	23095±96	27340±92	1.37±0.03
25	24742±75	1708±47	1.13±0.04	23398±111	2846±103	1.37±0.03
50	24896±35	1628±30	1.09±0.02	23547±46	2790±51	1.42±0.02
62	25071±35	1577±33	1.07±0.03	23717±40	2830±46	1.46±0.02
88	25243±33	1595±41	1.04±0.03	23888±31	2907±37	1.50±0.01
Hexane						
5	26227±14	1056±56	1.21±0.08	25021±37	2717±51	1.36±0.02
15	26247±16	1085±63	1.22±0.08	25037±39	2737±54	1.37±0.03
25	26253±19	1101±73	1.22±0.09	25034±45	2746±61	1.36±0.03
50	26259±29	1168±107	1.24±0.13	25044±63	2802±80	1.36±0.04
Isoprpyl Alcohol						
5	21198±239	3500±78	1.19±0.07	20818±29	2418±80	1.20±0.03
15	21268±274	3459±81	1.20±0.07	20872±32	2471±89	1.207±0.03
25	21360±351	3421±85	1.18±0.08	20935±37	2506±99	1.21±0.02
45	21568±327	3343±83	1.19±0.06	21028±27	2562±94	1.22±0.02
65	21607±211	3348±61	1.16±0.03	21132±41	2552±104	1.22±0.02
75	21300±22	3313±16	1.08±0.01	21444±22	2100±45	1.01±0.02
Propanol						
5	21490±346	3585±97	1.24±0.10	20818±9	2548±50	1.21±0.01
25	21513±370	3389±88	1.23±0.09	20904±14	2584±69	1.22±0.01
50	21604±310	3263±80	1.21±0.06	21006±21	2600±93	1.22±0.02
Decanol						
25	22256±239	3236±439	1.20±0.09	20971±42	2722±51	1.23±0.02
50	22425±598	2715±889	1.14±0.16	21064±60	2737±38	1.24±0.01
Butanol						
5	21572±308	3796±130	1.16±0.07	20604±6	2648±23	1.21±0.01
15	21409±424	3598±142	1.16±0.09	20633±9	2637±43	1.21±0.01
25	21458±422	3565±150	1.16±0.08	20700±10	2658±42	1.22±0.01
46	21613±517	3361±244	1.17±0.09	20802±23	2688±55	1.22±0.02
66	21829±368	3190±243	1.21±0.09	20888±52	2694±45	1.23±0.02
84	21874±673	3113±487	1.15±0.06	20965±57	2744±93	1.24±0.02
Octanol						
5	22311±168	3178±319	1.23±0.08	20872±31	2677±31	1.23±0.02
25	22035±277	3287±266	1.21±0.08	20920±42	2693±39	1.23±0.02
50	21979±382	3128±532	1.19±0.11	21013±96	2696±82	1.23±0.04

Table 3: Parameter values of fits to spectra in polar protic solvents and their 95 % confidence intervals. Excitation wavelength was 360 nm.

T (°C)	k_{mB} (cm^{-1})	width_B (cm^{-1})	ρ_B	k_{mA} (cm^{-1})	width_A (cm^{-1})	ρ_A
Isoprpyl Alcohol						
5	21198±239	3500±78	1.19±0.07	20818±29	2418±80	1.20±0.03
15	21268±274	3459±81	1.20±0.07	20872±32	2471±89	1.207±0.03
25	21360±351	3421±85	1.18±0.08	20935±37	2506±99	1.21±0.02
45	21568±327	3343±83	1.19±0.06	21028±27	2562±94	1.22±0.02
65	21607±211	3348±61	1.16±0.03	21132±41	2552±104	1.22±0.02
75	21300±22	3313±16	1.08±0.01	21444±22	2100±45	1.01±0.02
Propanol						
5	21490±346	3585±97	1.24±0.10	20818±9	2548±50	1.21±0.01
25	21513±370	3389±88	1.23±0.09	20904±14	2584±69	1.22±0.01
50	21604±310	3263±80	1.21±0.06	21006±21	2600±93	1.22±0.02
Decanol						
25	22256±239	3236±439	1.20±0.09	20971±42	2722±51	1.23±0.02
50	22425±598	2715±889	1.14±0.16	21064±60	2737±38	1.24±0.01
Butanol						
5	21572±308	3796±130	1.16±0.07	20604±6	2648±23	1.21±0.01
15	21409±424	3598±142	1.16±0.09	20633±9	2637±43	1.21±0.01
25	21458±422	3565±150	1.16±0.08	20700±10	2658±42	1.22±0.01
46	21613±517	3361±244	1.17±0.09	20802±23	2688±55	1.22±0.02
66	21829±368	3190±243	1.21±0.09	20888±52	2694±45	1.23±0.02
84	21874±673	3113±487	1.15±0.06	20965±57	2744±93	1.24±0.02
Octanol						
5	22311±168	3178±319	1.23±0.08	20872±31	2677±31	1.23±0.02
25	22035±277	3287±266	1.21±0.08	20920±42	2693±39	1.23±0.02
50	21979±382	3128±532	1.19±0.11	21013±96	2696±82	1.23±0.04

Table 4: Parameter values of fits to spectra in lipid bilayers and their 95% confidence intervals. Excitation wavelength was 360 nm.

T (°C)	width_B (cm^{-1})	width_R (cm^{-1})	ρ_B	ρ_R	$Area_B$	$Area_R$	k_{mB} (cm^{-1})	k_{mR} (cm^{-1})
DSPC								
15	1205±34	2843±8	1.02±0.03	1.24±0.01	0.075±0.005	0.925±0.008	23147±7.5	22448±13

37	1275±38	2895±8	1.03±0.03	1.22±0.01	0.067±0.005	0.887±0.009	23136±8	22436±13
51	1653±63	3229±21	1.20±0.03	1.20±0.01	0.119±0.014	0.772±0.023	23113±16	22273±28
52	1698±61	3272±22	1.19±0.03	1.20±0.01	0.131±0.014	0.764±0.024	23110±16	22235±30
53	1805±57	3393±25	1.20±0.03	1.17±0.01	0.167±0.016	0.717±0.026	23089±18	22103±35
54	2086±52	3706±26	1.21±0.03	1.07±0.01	0.237±0.013	0.612±0.022	23014±19	21570±37
55	2000±38	3725±31	1.05±0.02	1.00±0.01	0.121±0.006	0.668±0.007	23185±81	21061±16
56	2366±132	3354±79	1.06±0.04	1.05±0.02	0.130±0.020	0.622±0.020	23296±81	20711±42
57	2300±108	3350±79	1.02±0.04	1.05±0.02	0.116±0.016	0.626±0.016	23327±67	20713±31
58	2231±87	3382±55	1.00±0.03	1.04±0.01	0.102±0.012	0.630±0.013	23377±50	20720±22
59	2417±175	3299±86	1.05±0.05	1.05±0.02	0.119±0.022	0.605±0.022	23282±113	20663±47
DPPC								
5	1226±34	2783±9	1.00±0.03	1.23±0.01	0.079±0.005	0.920±0.008	23021±8	22294±13
25	1263±44	2835±10	1.04±0.04	1.22±0.01	0.076±0.006	0.963±0.010	23016±9	22281±15
35	1504±59	3086±17	1.12±0.04	1.21±0.01	0.096±0.011	0.826±0.019	23041±13	22201±26
39	1578±61	3171±19	1.14±0.04	1.20±0.01	0.111±0.013	0.792±0.021	23050±16	22141±30
40	1735±73	3234±28	1.17±0.04	1.18±0.01	0.148±0.019	0.747±0.031	23020±23	22061±41
41	1712±71	3252±25	1.18±0.04	1.18±0.01	0.139±0.017	0.728±0.028	23034±22	22064±38
42	1774±70	3283±36	1.16±0.04	1.17±0.01	0.160±0.019	0.684±0.031	23022±24	22004±43
43	1954±82	3476±45	1.21±0.04	1.12±0.02	0.213±0.022	0.707±0.036	22983±31	21777±51
44	2077±52	3595±75	1.07±0.02	1.00±0.01	0.145±0.009	0.696±0.011	23275±15	20954±21
45	2137±89	3533±75	1.08±0.025	1.00±0.01	0.144±0.017	0.681±0.017	23302±31	20889±34
50	2140±104	3456±73	1.04±0.04	1.01±0.02	0.117±0.016	0.681±0.017	23344±47	20779±29
60	2237±158	3340±75	1.02±0.06	1.03±0.02	0.088±0.017	0.637±0.018	23353±83	20661±31